A Radio System for Avoiding Illuminating Aircraft with a Laser Beam

W. A. COLES, T. W. MURPHY, JR., J. F. MELSER, J. K. TU, G. A. WHITE, K. H. KASSABIAN,
K. BALES, AND B. B. BAUMGARTNER

University of California, San Diego, 9500 Gilman Drive, La Jolla, CA 92093; bcoles@ucsd.edu, tmurphy@physics.ucsd.edu

ABSTRACT. When scientific experiments require transmission of powerful laser or radio beams through the atmosphere, the Federal Aviation Administration (FAA) requires that precautions be taken to avoid inadvertent illumination of aircraft. At present, the FAA requires that laser operators use human spotters to protect against accidental illumination. Here, we describe a simple, inexpensive, and highly reliable electronic system for detecting aircraft entering the vicinity of a laser beam that makes use of the air traffic control (ATC) radio transponders required on most aircraft. The radio system uses two antennas, both aligned with the laser beam. One antenna has a broad beam and the other has a narrow beam. The ratio of the transponder power received in the narrow beam to that received in the broad beam gives a measure of the angular distance of the aircraft from the axis that is independent of the range or the transmitter power. This ratio is easily measured and can be used to shutter the laser when the aircraft is too close to the beam. Comparisons of prototype systems operating at both the Apache Point and W. M. Keck Observatory with an FAA database indicate successful identification of commercial airplanes passing near the telescope boresight.

Online material: color figure

1. INTRODUCTION

A number of scientific experiments require the transmission of a laser beam through the atmosphere, using an astronomical telescope or its equivalent. Such experiments include lunar and satellite laser ranging (Dickey et al. 1994; Pearlman et al. 2002), creation of artificial guide stars for adaptive optics (e.g., Wizinowich et al. 2006), and atmospheric remote sensing using lidar (Measures 1984; Jelalian 1992). In order to avoid hazard to aircraft, the Federal Aviation Administration (FAA) requires that one or more observers be stationed outside any telescope that is transmitting a laser beam. These observers close the laser shutter when an aircraft is observed within 25° of the laser beam (as viewed from the telescope). In this article we discuss part of an aircraft detection system now employed at the Apache Point Observatory (APO) for a lunar ranging experiment called APOLLO (Apache Point Observatory Lunar Laser-ranging Operation; Murphy et al. 2008). A second system was successfully tested in the environment of Mauna Kea, and a new device is currently being prepared for the W. M. Keck Observatory. This system—dubbed the Transponder-Based Aircraft Detector (TBAD)—could be used not only for laser beam experiments as mentioned previously, but also for protecting aircraft from high-powered radar transmitters such as those used for ionospheric research (e.g., Folkstead et al. 1983). While no one technology is likely to satisfy every requirement for an aircraft avoidance system, we believe that the TBAD system could

function as the primary component of a multitier system— potentially complemented by optical or infrared imaging systems.

The transponder detection scheme is currently in place at APO in conjunction with a complementary infrared camera detection system, together providing robust detection of aircraft. The FAA recently commissioned a study of potential laser safety technologies (the committee was designated as G-10T), charged with establishing functional requirements for automated protection of aircraft from laser transmissions and defining criteria for system certification. The committee was briefed on the TBAD concept and performance demonstrations presented here. The TBAD technique satisfies the functional requirements outlined in the resulting SAE report (AS-6029) for airplanes equipped with operating transponders. The system has no difficulty detecting aircraft out to a slant range of 70 km; can tolerate close passes and high angular rates; and is not impeded by clouds, bright light, bats, insects, meteors, lightning, etc.

The FAA rules effectively require transponders on all commercial aircraft and most private aircraft (the exact language can be found in the Federal Aviation Regulations (FAR 91.215). These transponders are interrogated frequently (at 1030 MHz) by the regional ATC radars and also by the airborne Traffic Collision Avoidance System (TCAS). The transponders reply incoherently at 1090 ± 3 MHz with a pulse-coded response. The response must have vertical electric field polarization, an

omnidirectional pattern, and transmitted peak power between 70 and 500 W. Various coding schemes convey information about the aircraft. Mode-A and mode-C responses communicate a temporarily assigned aircraft identity and altitude, respectively. A newer mode-S encoding flexibly communicates permanent aircraft identity, coordinates, altitude, etc., but still as pulsed transmission at 1090 MHz. Mode-S transponders, which are used on all commercial and military aircraft, transmit once per second even when they are not being interrogated. Additionally, distance-measuring equipment on aircraft also transmit in the 1090 MHz band. In practice, we see combined mode-A and mode-C response rates from an individual aircraft around 10–20 per second over New Mexico and two–seven per second over Mauna Kea, never falling below 2 Hz over months of monitoring.

The primary failure mode for the TBAD technique is that a particular aircraft may not carry an operating transponder, could possibly be shadowed from the interrogator, or may be in a remote area without interrogation. Most airplanes capable of flying over high-altitude observatories will be equipped with transponders in order to legally fly over 10,000 feet above mean sea level. An exception is made for airplanes within 2500 feet of the ground, so that airplanes could, in principle, slip over even a high-altitude observatory above 10,000 feet without requiring a transponder. In any case, airplanes close to the terrain may not have line of sight to a ground radar station and thus may not receive interrogations. However, TCAS air-to-air interrogations practically ensure a high rate of interrogation activity over the continental United States and other locations with moderate air traffic density. Because the airplanes at risk of going undetected by the TBAD system tend to fly close to the ground, they will tend to be nearby and thus have a high angular rate. A complementary system must therefore be able to accommodate high-angular-rate aircraft. A thermal infrared camera system capable of detecting motion and triggering in less than 0.2 s is therefore a good match.

2. RADIO DETECTION DESIGN

The APOLLO laser is never used at elevations less than 15°, and this elevation restriction is typical of (if not much lower than) other laser and radar transmitters. Thus, for the maximum altitude of interest to the FAA standards—60,000 feet, or 18.3 km—the aircraft range will not exceed ∼70 km, and the received power is very high by modern communications standards (> -72 dBm) so that it may be easily detected with a total power receiver. However, the received power is highly variable because both the range and the transmitted power are variable. The design requirement is a highly reliable method of detecting when an aircraft transponder is within about 15° of the telescope beam. This 15° specification—differing from the 25° angle used by human spotters—is set by the expected angular rate of aircraft, transponder interrogation frequency, and

the desire to avoid excessive triggers when pointing the beam as low as 15° above the horizon.

The general concept is to use two antennas aligned with the optical axis of the telescope, one with a beam width (full width at half-power) of about 30° and the other with a beam width of about 90°, as shown in Figure 1. The ratio of the power received by the narrow-beam antenna to that received by the broad-beam antenna depends only on the angular position of the transponder with respect to the beam axis. In particular, it does not depend on the distance, transmitted power, or polarization mismatch.

The APO telescope, like many others used in this type of experiment, is on an altitude-azimuth mount with a secondary mirror more than 80 cm in diameter centered on the optical axis. The radio antennas can be mounted facing the sky on the secondary support structure and aligned with the optical axis without interfering with the optical beam, and the polarization will remain vertical as the telescope is moved. This geometry is also typical of the radar antennas used for ionospheric research, although the secondary reflector is much larger in these cases. For telescopes on an equatorial mount the position angle of the linear polarization changes with hour angle. This variation can be easily accommodated by changing to antennas that are sensitive to circular polarization.

The beam width of a planar antenna (in radians) is roughly the inverse of the width of the antenna (in wavelengths). Thus, the narrow-beam antenna must be wider than the broad-beam antenna. It is very attractive to design the narrow-beam antenna as an array of smaller antenna elements. In such an array the

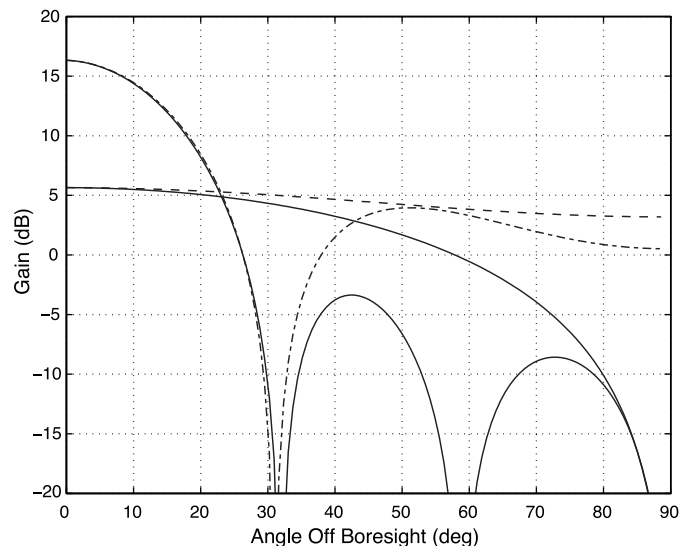FIG. 1.—Gain of the broad-beam and narrow-beam antennas as a function of the angular separation of the transponder from the axis. The solid lines are H-plane cuts through the gains of the antennas actually used and the dashed lines are E-plane cuts. If the antennas are pointed to zero elevation, the E plane is the vertical plane, and the H plane is horizontal. The power received is proportional to the gain.

signals received by all the elements are summed to produce one narrow-beam output. A single element by itself is suitable for use as the broad-beam antenna. In this case the ratio of the power received by the array to the power received by a single element depends only on the element spacing of the array and can be accurately calculated. The element spacing of the array can be adjusted to optimize the array beam width. A photograph of the seven-element hexagonal array of patch antenna elements mounted on the secondary support structure of the APO 3.5 m telescope is shown in § 6.

Patch antennas are well suited to be array elements in this application. A patch is simply a half-wavelength square of copper foil on the top of a thin dielectric board with a ground plane on the bottom. It is connected through a post from under the ground plane. Patches have a narrow bandwidth, which is a significant advantage in this case, because it helps eliminate interfering radio signals. They are also very robust mechanically—another significant advantage in this application. The polarization of a patch can be changed from linear to circular simply by moving the connection post and changing the width of the patch slightly.

The system design consists primarily of impedance matching a simple patch antenna at 1090 MHz, adjusting the array configuration to obtain a suitable beam width and adequately low sidelobes, designing total power detectors for the two channels, development of signal processing electronics, and devising a reliable calibration system. A block diagram of the analog signal flow is shown in Figure 2. Here, one can see that we have used the center element of the array both as an array element and as the broad-beam antenna by splitting the signal with a power divider. To compensate for that power division, the other array elements must have -3 dB (half-power) attenuators before the array summer.

3. PATCH DESIGN

We used a simple square patch excited by a post, fed by coaxial cable from behind the ground plane. As the desired electric field polarization is vertical, the feed post must be centered in the horizontal coordinate and offset in the vertical coordinate,

as shown in Figure 2. Should circular polarization be desired, the feed point would be moved to the corner and the horizontal and vertical widths would be made a few percent different. The resonant frequency is set by the vertical width of the patch. The impedance is determined primarily by the feed position and to a lesser extent by the horizontal width. We wanted to make the patch using 60 mil dielectric circuit board material, as such a patch has about the bandwidth we need. We tested a patch made with the widely used FR4 circuit board material, finding that about half the received power is absorbed by the dielectric. This dielectric loss also doubles the bandwidth. To avoid broadening the bandwidth and reducing the gain we used a new low-loss laminate (Rogers RO4535), which has a loss tangent about 10% of that of FR4. With this material the dielectric loss was a small fraction of the received power.

This is a very simple patch design, so we did not use an electromagnetic simulator. We calculated the gain and impedance by modeling the patch as a pair of slots over an infinite ground plane connected by a microstrip transmission line with a lossy dielectric. We had to trim the final design by a few percent after fabrication. The final dimensions were $W_x = 71.0$ mm and $W_y = 70.2$ mm, and the feed point was 23.3 mm above the lower edge. The ground plane occupied the entire back surface of the 105 mm square dielectric, so that the ground plane fabricated onto the antenna extended approximately 17 mm beyond the patch boundaries. The calculated gain for an infinite ground plane was 5.3 dBi, which includes a dielectric loss of 0.5 dB. The measured gain for a patch mounted on a large ground plane was 4.7 ± 0.5 dBi, which is a reasonable agreement. The impedance was measured for four different ground planes and is shown in Figure 3. A ground plane extending 51 mm past the antenna (a total of 68 mm beyond the patch) is indistinguishable from a much larger ground plane.

The extent of the ground plane is an important factor, as it will often be convenient to minimize the weight and windage of the ground-plane material. In the presence of the full array ground plane there is essentially no back radiation. However, with a reduced ground plane there will be some back radiation
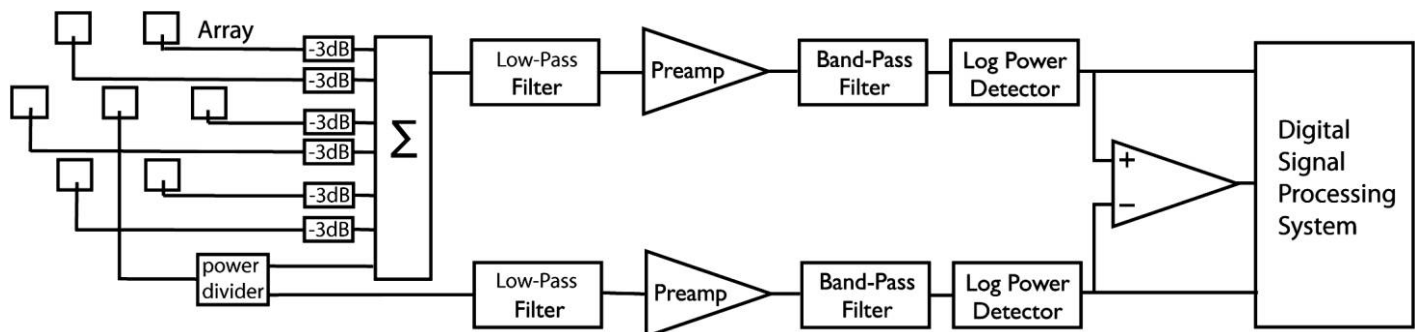

FIG. 2.—Block diagram of the analog signal flow. The patches are shown with the E field vertical. The azimuthal angle is defined with respect to the horizontal. The array is drawn approximately to scale. The center patch is used both as an array element and as the broad-beam element.
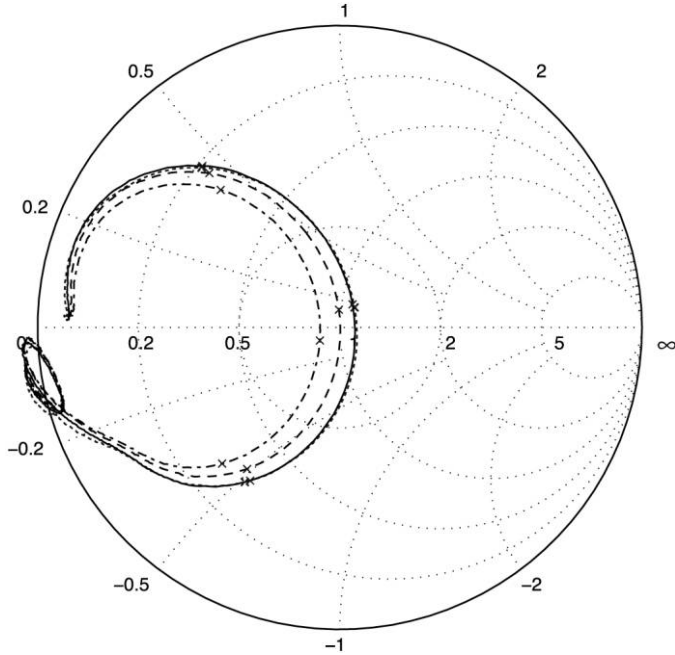
FIG. 3.—Measured driving point impedance of the patch with various ground planes shown on a Smith chart. This is a polar plot of reflection coefficient. A reflection coefficient inside the inner concentric circle that passes through 0.5 and 2.0 defines the passband. The normalizing impedance is 50Ω. The "x" symbols are at 1080, 1090, and 1100 MHz. The inner dash-dotted trace is the patch antenna as fabricated, for which the ground plane and dielectric extends 17 mm around the patch. The dashed trace is for the antenna mounted on an aluminum plate that extends a further 17 mm around the antenna exterior. The dotted trace is for an aluminum plate that extends 51 mm around the antenna, quadrupling the original ground-plane extent. The solid trace, largely overlapping the dotted curve, is for a large plate used to mount the entire array.

and some change in impedance. Accordingly, we measured the impedance and the front-to-back ratio of a single patch with different ground-plane widths. The front-to-back ratios of the three smaller ground planes shown in Figure 3 were 9 dB, 13 dB, and 22 dB. On the basis of these measurements we decided that a 50 mm aluminum border around the antenna was adequate.

The beam of the patch $G_P(\theta, \phi)$ is relatively broad. An H-plane cut through $G_P(\theta, \phi)$ has $\sin^2(\theta)$ behavior, as shown in Figure 1 with a solid line. The pattern is broader in the E-plane (shown dashed in Fig. 1), dropping only 2.4 dB at 90°. We did not attempt to measure the beam width because a measurement without an adequate test range would be no better than our calculation, and the exact pattern of the patch is unimportant to our design because it factors out of the *ratio* of the array gain to the patch gain.

4. ARRAY DESIGN

The array must have a beam width of about 30° and sidelobes at least 10 dB below the main beam. The array will be mounted

with its normal aligned to the optical axis, and the array elements will all be equally phased so that the beam is normal to the array plane. The purpose of the array is to create a narrow beam, which can be compared with the broader beam of a single element, to determine the angular separation of the transponder from the telescope optical axis. Thus, we are not concerned with the gain of the array as much as the ratio of its gain to that of a single patch (R). The gain of the single patch factors out of this ratio, simplifying the calculation. The design problem then is to adjust the patch configuration to obtain an optimal ratio R.

The gain of the array $G_A(\theta, \phi) = C \times G_P(\theta, \phi) \times AF(\theta, \phi)$. The constant C is determined such that the integral of G_A over all space is 4π. The array factor AF is given by

$$\text{AF}(\theta, \phi) = \sum_{i=1}^{n} W_i \exp(-j\mathbf{k}(\theta, \phi) \cdot \mathbf{B}_i).$$

Here, $\mathbf{B}_i$ is the vector location of the ith patch, W_i is the (complex) excitation of the ith element, and $\mathbf{k}(\theta, \phi)$ is the wave vector for a plane wave arriving at the array from the direction defined by (θ, ϕ). The desired ratio $R = C \times \text{AF}$. Of course, one must also allow for the gains of the amplifiers, losses in the cables and summing junction, etc.

We searched the space of symmetrical equally weighted arrays ($W_i = 1$) with $n = 6$, 7, and 9 to find a suitable $\text{AF}(\theta, \phi)$ with the minimum n. We found a good fit to our requirements with a hexagonal configuration of $n = 7$ elements. The pattern has a six-part symmetry in azimuth, with sidelobes at two phases. We have defined zero azimuth to be the horizontal, as shown in Figure 2. The sidelobes have equal amplitude when the element
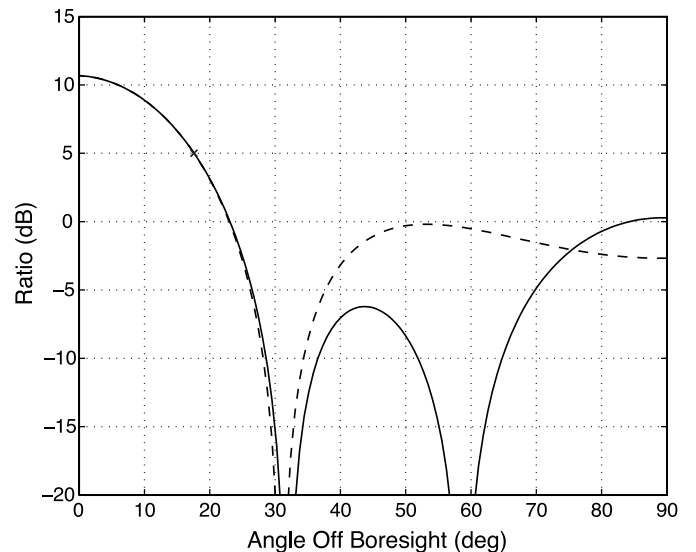

FIG. 4.—Cuts through $R = C \times AF(\theta, \phi)$ at azimuths $\phi = 0°$ (*solid line*) and 90° (*dashed line*), corresponding to the highest sidelobes. The "x" marks a robust detection threshold for concluding that an aircraft is too close to the beam axis.

spacing is 0.82λ. The peak-to-sidelobe ratio is 11 dB. Cuts through the ratio R at azimuths of $0°$ (the H plane) and $90°$ (the E plane), which correspond to the highest sidelobes, are shown in Figure 4. A detection threshold $R > 5.5$ dB provides the greatest error margin. This corresponds to an angle of $17°$ off the axis—close to the design goal and somewhat conservative.

The patch antennas were mounted on an aluminum plate to provide accurate location, and the summer was mounted on the same plate. The plate provides a ground plane, but it is not essential that the ground plane be continuous, provided that the ground extends 50 mm past each antenna. The outer boundary of the mounting plate was trimmed to provide just the necessary 50 mm of extent. Slots were also cut within the mounting plate where possible, to reduce the windage.

We did not expect much mutual coupling with the spacing of 0.82 wavelengths, but we measured the magnitude of S_{ij} between the elements. We found it was -27 dB between colinear elements and -31 dB between diagonal elements. We also measured the driving point impedance of the center element with all other elements open and also with all other elements loaded. We could not detect any deviation from the impedance of an isolated element with a ground plane more than 50 mm around the element.

We did not attempt to measure the pattern of the array because, with negligible mutual coupling, the calculation is more accurate than any measurement we could make. However, we did measure the gain at the beam center. The calculated array gain is 16.3 dBi and the measurement was 15.95 ± 0.5 dBi—quite a reasonable agreement.

5. RECEIVER DESIGN

The APOLLO laser is never operated at an elevation less than $15°$, because the accuracy of the lunar ranging is degraded at low elevations by reduced throughput and atmospheric fluctuations. Thus, the greatest range one can expect for aircraft flying 15 km above the site (itself at 2.8 km altitude) is 60 km. The gain of a single patch is about 4.7 dB, so the signal level from the minimum-power transponder will be at least -70 dBm. At a distance of 1 km the signal level would increase to about -35 dBm. At the minimum reasonable distance of 100 m, the signal level would be about -15 dBm.

The signal level is so high that the noise figure of the preamp is not a factor, but interference from the cellular communications band near 900 MHz can be very strong. Although the patch antenna has a -3 dB bandwidth of $\approx 1\%$, it does not reject a signal at 900 MHz by more than about -20 dB. Thus, a multipole bandpass filter is required. Fortunately, suitable filters are available off the shelf. We used a five-pole ceramic filter No. 930644 from the International Microwave Corporation. We also used a sharp-cutoff low-pass filter to reduce the interference from various communications above 2 GHz. Because the signal level is so high, we split the signal from the center array element and used it both for the array and for the

broad-beam single element. To compensate for the 3 dB loss we inserted 3 dB attenuators in the path from the other elements to the beam former, as pictured in Figure 2.

There are a number of inexpensive log amplitude detectors with good accuracy and wide dynamic range. These are particularly attractive because the log of the desired power ratio R can be obtained simply using a differential amplifier to subtract the log of the broad-beam power from the log of the narrow-beam power. We used part number $ZX47 - 60+$ from Mini-Circuits Lab with a dynamic range of 5 dBm to -60 dBm. To match this to the expected signal levels, we used a preamplifier with a gain of about 38 dB before the power detector. The only requirement on the preamp is that it have relatively low bias current, because it is important to minimize the power dissipated near the optical axis of the telescope to avoid image degradation arising from air turbulence. The output of the detectors need only pass the narrowest transponder pulse of 450 ns. We used a third-order Butterworth low-pass filter with a 100 ns time constant to minimize the postdetection noise.

6. SIGNAL PROCESSING

The signal processing unit performs the dual function of deciding when to close the laser shutter and capturing the pulse code for logging aircraft identities and altitudes. An example
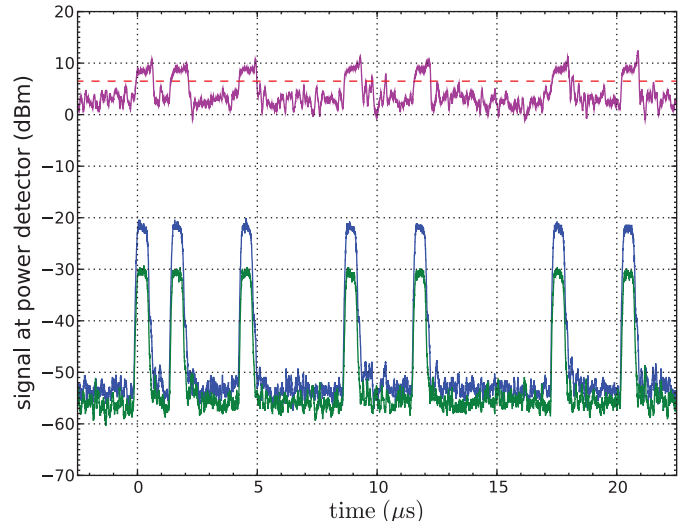

Fig. 5.—Example pulse train obtained in San Diego, showing both the broad antenna signal (*green*) and the directional signal (*blue*), as well as the output of the difference amplifier (*magenta*). The two antenna signals are represented as postamplifier power at the power detector, while the difference signal is represented as the ratio, in decibels. The pulse pattern decodes to 4530, which could either be a mode-A identity or a mode-C altitude (corresponding to an altitude of 3400 feet). In this case, the directional signal is stronger than the broad signal, indicating that the source is within the primary beam of the directional array. The red dashed line shows where one might place a threshold for judging in-beam activity. The trailing-edge spikes are not uncommon and motivate using only the first part of the pulse for discrimination, as discussed in the text.

pulse pattern is shown in Figure 5. The decision to close the shutter is based on four criteria, any of which—when satisfied—will result in laser closure:

    1. D1 = DIREC/BROAD ratio $R > 5.5$ dB, AND DIREC signal > -24 dBm at detector.
    2. D2 = DIREC signal > -4 dBm at detector.
    3. D3 = BROAD signal > -4 dBm at detector.
    4. D4 = |supply current − nominal| $> 0.05 \times$ nominal.

The first criterion is the most important, representing the directionally sensitive detection mode. The second criterion avoids a failure mode of the first criterion due to saturation of the DIREC signal from a nearby source. The third criterion prevents a nearby, fast-angular-motion airplane from getting into the protected zone before the other two criteria are activated—keeping in mind that we rely on external interrogation occurring before sensing the presence of the aircraft. Each of these decisions is based on comparators sensing the outputs of the logarithmic power detectors and referenced to an adjustable voltage, with the DIREC/BROAD ratio provided by a difference of the logarithmic outputs. The angular size of the protected zone on the sky is adjustable by setting the difference-comparator reference voltage.

The criteria based on signal levels map into different nominal ranges for the three different peak power requirements imposed by the FAA. For noncommercial traffic (typically low-altitude), the minimum peak power requirement is 70 W. For commercial aircraft, the minimum requirement is 125 W. The maximum allowable peak power is 500 W. Figure 6 illustrates the distances to which the first three criteria in the preceding list apply for the three limiting cases of transmitted power. For example, an airplane with a 125 W transmitter will saturate the broad antenna channel (criterion 3) if within 1.9 km; will saturate the directional channel (criterion 2) within 3.2 km to 5.4 km, depending on where it is within the directional beam; and will be protected by the "in-beam" criterion (the first in the list) out to 55 to 92 km, depending again on beam position.

Any of the three triggers activates a retriggerable one-shot, holding the laser shutter in a closed condition for 5 s. Reaction time is within 30 μs of signal receipt. The system is not confused by multiple aircraft in the beam at the same time. Any signal deemed to meet the preceding criteria will activate the shutter. The signal processing unit also monitors the power supply current to ensure that the components are operating normally before allowing the laser shutter to open.

The signal processing unit also captures the altitude and identity codes transmitted from aircraft that have triggered shutter closure, for the purpose of recording activity. This is done using a PIC microprocessor responding to the initial pulse via an interrupt service routine, then checking at regular intervals (about 1.45 μs) for any pulse transitions within the previous pulse period. Though coded to interpret mode-A (identity) and mode-C (altitude) responses, the characteristic pattern of mode-S transmissions can be discerned, and distance-measuring equipment
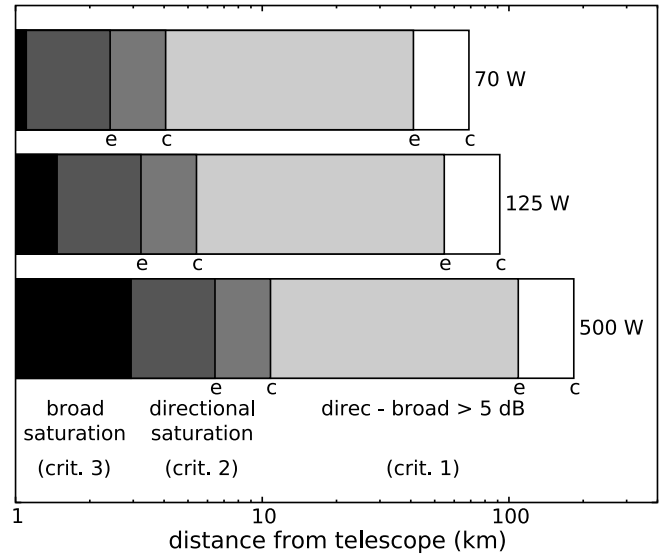

FIG. 6.—Protected line-of-sight ranges for the first three shutter closure criteria described in the text for three different transmitter powers corresponding to: 70 W—the minimum for noncommercial (typically low-altitude) aircraft; 125 W—the minimum for commercial aircraft; and 500 W—the maximum power permitted. For each, the zone for which the broad channel saturates is black; the zone for which the directional channel saturates is medium gray; and the zone in which the ratio criterion is relied upon is a light shade. For the latter two, different shadings represent response at the edge and center of the 15° half-width protected area on the sky, denoted by "e" or "c," respectively.

(DME) signals operating on the same transmit frequency band can also be identified. Note that any signal meeting the criterion established previously will close the laser shutter, regardless of information content. The information is used to build a database of the frequency and nature of the aircraft-caused triggers—including a crude estimate of distance, given telescope elevation angle and aircraft altitude. The microprocessor can also assume control of the shutter and build in false-trigger avoidance. Electrostatic discharge or lightning generally produces a single pulse, while aircraft signals (mode-A, mode-C, mode-S, and DME) all contain multiple pulses within 20 μs. These "glitches" may be ignored.

We have found that multipath interference—especially seen by the broad-beam antenna—often compromises the pulse quality and often produces false triggers. We have successfully tested a method to mitigate such false triggers, by applying preceding criterion 1 only during a 50 ns window shortly following the leading edge of a clean pulse (one that has only background noise preceding it). We have seen this approach dramatically reduce the number of false in-beam triggers while not compromising the robust detection of true in-beam events.

Besides the check that the current delivered to the electronics is good, the microprocessor sends a keep-alive packet once per minute to assure system health. It is straightforward to verify that the system is operational before commencing with laser

activities. Logged information is sufficient to verify sensitivity to aircraft on a nightly basis, but an in-dome calibrated transmitter may also be useful to verify proper sensitivity.

The TBAD system is implemented as three physical units, all designed and built at the University of California, San Diego (UCSD). The antenna array and passive summing devices are mounted to a single aluminum plate 0.63 m across that also serves as an extended ground plane. The RF processing and discrimination is performed in a small electronics enclosure measuring $22 \times 15 \times 6$ cm^3 that is located close to the antenna. These electronics only consume 3 W of power, so that the box may be safely deployed in front of a telescope without disrupting image performance. The microprocessor and power supply occupy a second box measuring $19 \times 12 \times 8$ cm^3 that may be located tens of meters from the antenna RF electronics. A connection from the microcontroller box to a computer or terminal server completes the system. Figure 7 shows the antenna mounted on the 3.5 m telescope at APO, on the sky-facing side of the secondary mirror support structure.

7. PERFORMANCE

The prototype TBAD system was deployed on the Apache Point Observatory 3.5 m telescope on 2008 December 19 for initial characterization—without the authority to shutter the laser. It was operated whenever the telescope enclosure shutter was open, regardless of whether the laser was in use. Note that the solid angle of visible sky is restricted by the enclosure to a range of 1.9–2.7 sr, depending on telescope elevation angle, averaging only 36% of the sky. For testing purposes we recorded all aircraft detected by the broad-beam antenna, setting the detection threshold to sense airplanes within 20 km at 70 W

peak power, or 52 km at 500 W. We detected an average of six aircraft per night, with a maximum of 20, during 72 full nights from 2008 December 31 to 2009 August 7. Of these detections, an average of two per night—with a maximum of nine—were in-beam and (would have) shuttered the laser. The mean observing time per night was 42,000 s, for which a median of 70 s, with a maximum of 283 s, was shuttered (~0.2% closure). Thus, at APO shuttering the laser causes an insignificant loss of observing time, and these results match the experience of human spotters.

When an aircraft is detected in-beam there are many "detection" events, because its transponder operates continuously. Typically, we see 12 events per second during the time the aircraft is in-beam. Of these, about 40% are associated with mode-A identity codes, 35% with mode-C altitude codes, 20% with DME pulses, and 5% are identified as mode-S information packets. We decode and record the mode-A and mode-C information, but do not decode the mode-S information with the present firmware. Figure 8 demonstrates the behavior of a typical beam-crossing detection. The metal telescope enclosure shields the antenna from line-of-sight detection at large angles, which results in a relatively tight truncation of the sequence. In this case, the central beam crossing was robustly detected in 408 events, roughly centered in the crossing of the open enclosure slit.

A comparison with five nights of Performance Data Analysis and Reporting System (PDARS) flight track data provided by the FAA showed two flight tracks crossing the telescope line
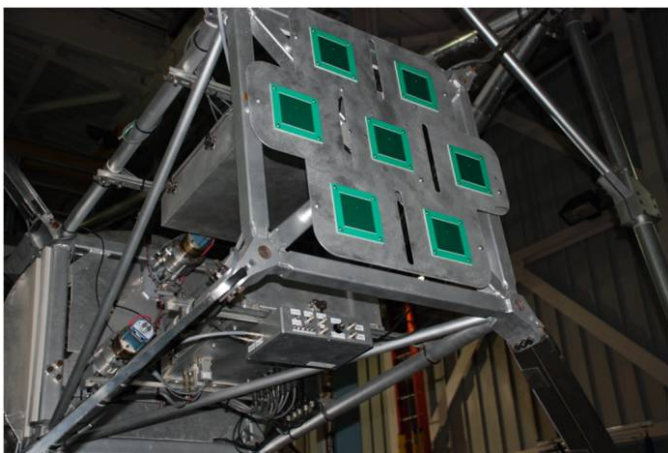

FIG. 7.—The antenna array mounted on the sky-facing side of the secondary mirror support structure on the APO 3.5 m telescope. The electronics box with white labels visible below the antenna plate contains the RF electronics, and consumes only 3 W of power.See the electronic edition of the *PASP* for a color version of this figure.
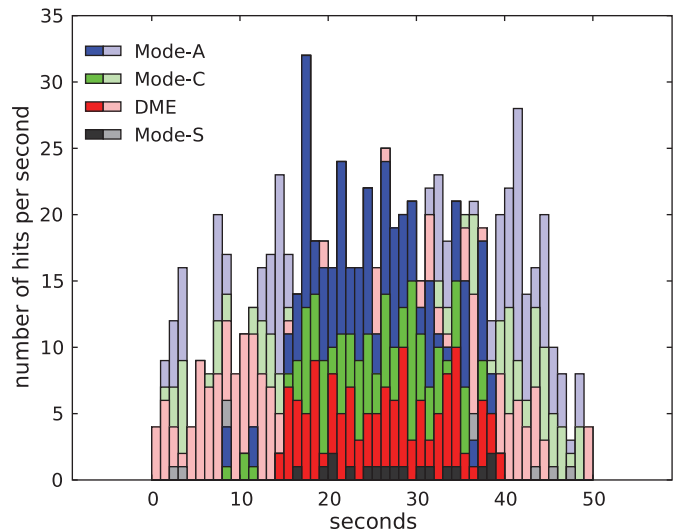

FIG. 8.—Event rate in 1 s bins for a pass acquired on 2008 December 31, for an airplane squawking identity code 6755 at an altitude of 39,000 feet, while the telescope was at an elevation angle of 54°. Event types are coded as blue for identity (mode-A), green for altitude (mode-C), red for DME, and black for mode-S. Saturated shades represent those detections deemed to be in the central beam by criterion 1 in § 6.

of sight. The transponder detector identified both aircraft as beam-crossers and would have shuttered the laser. Many other airplanes were sensed and recorded, but did not cross into the protected zone.

While the first prototype was being tested at APO we continued to test the second prototype on the UCSD campus, which is in a very heavy air traffic environment. San Diego International Airport is 17 km south of UCSD, and Miramar Naval Air Station is 5 km east. Furthermore, our laboratory building is in a highly "built" urban environment with many potential radio scattering objects visible from the roof. When the antenna was pointed 25° above the horizon toward the San Diego International Airport, the shutter was closed 40% of the time—and 80% during the busiest hours of the day, even though aircraft could rarely be seen in the beam. It was clear that there was a problem of "false detection" of in-beam events. We found that, unlike the APO tests, many in-beam events were not observed continuously during the time that the aircraft was (supposedly) in beam. A close inspection of the received pulses showed that false detections were often caused by multipath interference in the broad-beam antenna channel.

Multipath interference can either reduce or increase the integrated pulse power, depending on the phase of the reflection. However, the power can be increased to no more than twice the incident power, whereas it can be reduced to zero. Since multipath is primarily in the broad beam, it can at most decrease the ratio of narrow to broad by a factor of 2, whereas the ratio may increase to arbitrarily large values. Thus, false detections are far more common than detection failure.

We revised the detection algorithm using two characteristics of multipath interference. First, multipath involves a significant time delay, so the leading edge of a pulse is unaffected by the reflection. We took advantage of this property by measuring the power only during the first 50 ns of each pulse. This reduced the shuttered time from the 40% mentioned previously to about 7%. Second, we took advantage of the sporadic nature of multipath, accepting as real in-beam events only those that occurred more than 10 times in a 5 s interval. We only apply this condition to the first criterion in the preceding list and can adjust the number of events required for action. This filter reduced the shuttered time to about 3%. As we adjusted the parameter to require a greater number of in-beam events per 5 s interval, we were unable to reduce the closure time below about 2%. This suggests that aircraft were actually in beam about 2% of the time, and this rate is consistent with the air traffic environment. Zenith pointings at UCSD resulted in shutter closures 3% of the time without the leading-edge window filter, 0.4% with the filter, and 0.1% of the time with the additional software filtering activated. Observatories tend to be in far less congested areas, so that these interference issues—while manageable—will be less important. These improvements in false-detection rate have not impacted the TBAD's ability to discriminate true events within the protected beam.

After testing at UCSD, and a brief deployment on the Palomar 200 inch telescope in late 2009, we shipped the second prototype antenna to be tested in the environment of Mauna Kea in Hawaii. Over a period of about 75 days, the antenna was pointed in a variety of directions from a position on the roof of the building between the two Keck 10 m telescope domes. A simultaneous campaign using the Flight Explorer air traffic platform logged nonmilitary flight activities in the region. This allowed a direct comparison of transponder detections to 3-D flight paths. From this campaign, we determined the following:

1. The TBAD system saw every Flight Explorer track within the probed airspace for each pointing.

2. The TBAD system detected activity not reported by Flight Explorer on eight of the zenith-pointing test days. These episodes had the characteristics of military activity.

3. There were no instances of false detections.

4. Event rates were always over two events per second at every time of day or night and for any trajectory within the airspace.

5. Typical event rates were three per second, or five per second when including DME activity (which is equally capable of triggering the in-beam flag).

6. The TBAD system is capable of detecting aircraft well beyond the range requirement for protection to 60,000 feet altitude at elevation angles as low as 15°.

7. Overhead traffic was too sparse to generate a beam-crossing event at realistic observing altitudes during the test period. Except for a horizon-pointing capturing the departures and arrivals from the Hilo airport, no beam-crossing events were detected in this environment.

The results of these tests encouraged the staff at the W. M. Keck Observatory to commission the installation of a new antenna fabrication on the telescope—likely to be completed by early 2012. The functional requirements outlined by the G-10T committee favor the adoption of this technology by the FAA, which is being actively pursued by the Keck staff.

REFERENCES

Dickey, J. O., Bender, P. L., Faller, J. E., Newhall, X. X., Ricklefs, R. L., Ries, J. G., Shelus, P. J., Veillet, C., et al. 1994, Science, 265, 482

Folkestad, K., Hagfors, T., & Westerlund, S. 1983, Radio Sci., 18, 867

Pearlman, M. R., Degnan, J. J., & Bosworth, J. M. 2002, Adv. Space Res., 30, 135

Wizinowich, P. L., Le Mignant, D., Bouchez, A. H., Campbell, R. D., Chin, J. C. Y., Contos, A. R., van Dam, M. A., Hartman, S. K., et al. 2006, PASP, 118, 297

Measures, R. M. 1984, Laser Remote Sensing: Fundamentals and Applications (New York: Wiley)

Jelalian, A. V. 1992, Laser Radar Systems (Boston: Artech House)

Murphy, T. W., Adelberger, E. G., Battat, J. B. R., Carey, L. N., Hoyle, C. D., Leblanc, P., Michelsen, E. L., Nordtvedt, K., et al. 2008, PASP, 120, 20